ARTICLES

Journal of Semiconductors
(2020) 41, 032305
doi: 10.1088/1674-4926/41/3/032305

Analysis of the time domain characteristics of tapered semiconductor lasers

Desheng Zeng[1, 2], Li Zhong[1, †], Suping Liu[1], and Xiaoyu Ma[1, 2]

[1]National Engineering Center for Optoelectronic Device, Institute of Semiconductors, Chinese Academy of Sciences, Beijing 100083, China
[2]University of Chinese Academy of Sciences, Beijing 100049, China

Abstract: We use traveling wave coupling theory to investigate the time domain characteristics of tapered semiconductor lasers with DBR gratings. We analyze the influence of the length of second order gratings on the power and spectrum of output light, and optimizing the length of gratings, in order to reduce the mode competition effect in the device, and obtain the high power output light wave with good longitudinal mode characteristics.

Key words: tapered semiconductor lasers; time domain characteristics; DBR gratings; mode competition

Citation: D S Zeng, L Zhong, S P Liu, and X Y Ma, Analysis of the time domain characteristics of tapered semiconductor lasers[J]. *J. Semicond.*, 2020, 41(3), 032305. http://doi.org/10.1088/1674-4926/41/3/032305

1. Introduction

Semiconductor lasers have compact structure, high photoelectric transformation efficiency and wide range of lasing wavelengths, so they have great application prospects in optical communication, laser processing, laser ranging, biomedical equipment and so on[1–3]. Single chip integrated tapered semiconductor lasers can amplify the power of wave mode from the seed light source, obtaining higher output power with little effect on beam quality. Their fabrication is simple and the fabrication cost is low. Consequently, they have become one of the research hot-spots of laser technology. Paschke and Sumpf *et al.*[4] have found that using different electrodes to separately drive the master area and amplify area can obtain high power and nearly diffraction limited output laser. Since a DBR laser with first order gratings emits two degenerate modes, there are lobes in the far field. However, the second order gratings produce two order diffraction, corresponding to the grating coupling and the surface emission loss. Surface emission loss can cause a large threshold gain difference between the main mode and the lowest order mode, which eliminates pattern degeneracy. Consequently, second order gratings are used to improve the mode characteristics[5].

In this paper, we use traveling wave coupling theory to investigate the time domain characteristics of tapered semiconductor lasers with second order DBR gratings[6], which it is separately driven by two different electrodes. The tapered laser structure, as shown in Fig. 1, is divided into four sections, as follows: the master-oscillator (MO) region, with a length of L_2 and a width of 4 μm; the rear grating, with a length of L_1; the front grating region, with a length of L_3; and the second order grating[7], whose the coupling coefficient is κ and surface emission loss is ε. The front and back gratings play significant roles in determining the stability and operating characteristics of the device. Typically, the longer front grating provides additional isolation from the residual facet reflections and lowers the facet anti-reflection coating requirements. The duty cycle is 0.3 and the tapered amplify region with a length of L_4 and a flare angle of about 6°[8]. R and S represent forward wave and backward wave, respectively.

In the following section, the traveling wave theory and coupled mode equation are introduced and the finite difference method is used to solve the equation. In the third section, the simulation results are given, the variation of output optical power and charge carriers with time of tapered laser with DBR grating is analyzed, and the influence of different length front grating on longitudinal mode characteristics is compared. In the last section, the work of this paper is summarized.

2. Method

In semiconductor lasers with second order gratings, the coupling of the front and rear traveling waves must be considered. In this paper, $R(t, z)$ stands for the forward wave, $S(t, z)$ represents the backward wave, and the time domain coupling wave equation that they satisfy is as follows[9–11]:

$$\left(\frac{1}{v_g}\frac{\partial}{\partial t}+\frac{\partial}{\partial z}\right)R=[g-a-\varepsilon(z)]R+[i\kappa(z)-\varepsilon(z)]S+\Phi_R, \quad (1a)$$

$$\left(\frac{1}{v_g}\frac{\partial}{\partial t}-\frac{\partial}{\partial z}\right)S=[g-a-\varepsilon(z)]S+[i\kappa(z)-\varepsilon(z)]R+\Phi_S, \quad (1b)$$

where v_g represents the group velocity of the light wave, g represents the amplitude gain and phase change of the active region, a represents the energy loss caused by free carrier absorption and scattering, the value in MO area is a constant: the value of a_0 in this paper is 2 cm^{-1}, in the tapered amplify area, $a=a_0+\frac{1}{2r}$ (r is the curvature radius of the current light field), ε represents radiation loss caused by gratings, κ is the grating coupling coefficient, ε and κ are zero away from the grating area. The output power is the product

Correspondence to: L Zhong, zhongli@semi.ac.cn
Received 24 MAY 2019; Revised 17 OCTOBER 2019.

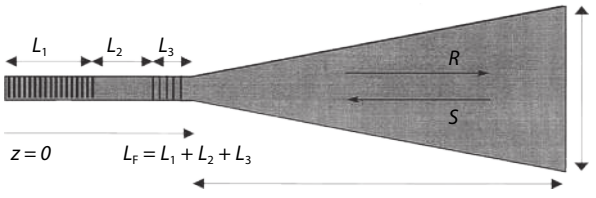

Fig. 1. Schematic top view of the laser.

of the square of output light intensity $|R|^2$ and the lateral width of the field W. Gain g is a function of time t and position z, and the expression is as follows:

$$g(t,z) = \frac{G(z,t)}{2}(1 - i\alpha), \tag{2}$$

where α is the line-width enhancement factor, the expression of $G(z,t)$[12] is as follows:

$$G(z,t) = A(N(z,t) - N_0), \tag{3}$$

where A is the differential gain coefficient, $N(z,t)$ is the carriers sheet density, N_0 is the transparency sheet density. The last term of the coupled wave equation Φ_R and Φ_S represent the contribution of spontaneous emission to the light field[13,14], and the expression is as follows:

$$\langle \Phi_i(z,t)\Phi_i(z',t')\rangle = \delta(z-z')\frac{\pi\Delta\upsilon}{2}\mathrm{e}^{-\pi\Delta\upsilon|t-t'|} \times (Gn_{\mathrm{sp}}(z)h\nu\frac{w_{\mathrm{act}}}{W^2}), \tag{4}$$

where i represent R and S. The product of the upper formula and the lateral width W of the light field is the ratio of spontaneous emission to the forward wave or the backward wave. $\Delta\upsilon$ corresponds to the full-width at half-maximum of the Lorentzian line-shape function, which is associated with the direct electron and hole radiative transition. Hence, $\frac{\pi\Delta\upsilon}{2}e^{-\pi\Delta\upsilon|t-t'|}$ in the Eq. (4) can be reduced to a delta function, $\delta(t-t')$, w_{act} is the width of active layer, n_{sp} is spontaneous emission factor, whose expression is:

$$n_{\mathrm{sp}}(z) = \frac{1}{1 - \exp\{[h\nu + E_{\mathrm{FV}}(z) - E_{\mathrm{FC}}(z)]/k_{\mathrm{B}}T\}}. \tag{5}$$

As can be seen from this formula, n_{sp} varies with the change of position z. For many applications, the incomplete inversion factor is adequately treated as a constant.

The time and spatial distribution of the carrier sheet $N(t,z)$ is as follows:

$$\frac{\partial N(z,t)}{\partial t} = \frac{\eta_i}{e}J(z,t) - \Re(N) - \frac{G}{h\nu}(|R|^2 + |S|^2), \tag{6}$$

where η_i is the injection efficiency, $J(z,t)$ is the density of current, $\Re(N) = \frac{N(z,t)}{\tau_{\mathrm{e}}}$ represents non-radiation loss, τ_{e} is equal to the recombination lifetime.

Next, the finite difference method is used to solve the Eqs. (1a), (1b) and (6). Before that, the difference recurrence relation must be derived. Let $t = k\Delta t$, $z = m\Delta z$, $R(t,z) = R(k,m)$, $S(t,z) = S(k,m)$, $N(t,z) = N(k,m)$, chooses approximate Δt, makes it satisfy the correlation: $\Delta t = \Delta z/v_g R$ satisfies the recurrence relations[15]:

$$\begin{aligned} &R(t+\Delta t, z+\Delta z) - R(t,z) \\ &= R(t+\Delta t, z+\Delta z) - R(t, z+\Delta z) + R(t, z+\Delta z) - R(t,z) \\ &= \frac{\partial R}{\partial t}|_{z+\Delta z}\Delta t + \frac{\partial R}{\partial z}|_t \Delta z \\ &= \frac{\partial R}{\partial t}|_{z+\Delta z}\Delta t - \frac{\partial R}{\partial t}|_z \Delta t + \frac{\partial R}{\partial t}|_z \Delta t + \frac{\partial R}{\partial z}|_{\Delta t}\Delta z \\ &= \frac{\partial^2 R}{\partial z^2}v_{\mathrm{g}}\Delta t\Delta z + \left(\frac{1}{v_{\mathrm{g}}}\frac{\partial R}{\partial t} + \frac{\partial R}{\partial z}\right)\Delta z. \end{aligned}$$

According to the slowly varying envelope approximation, the second order reciprocal of R to z can be ignored, and the following recurrence relation can be obtained:

$$R(k+1, m+1) = R(k,m) + \Delta z\Psi_R, \tag{7a}$$

where Ψ_R represents all terms on the right side of Eq. (1a). Similarly, we can deduce the recurrence relationship about S:

$$S(k+1, m-1) = S(k,m) + \Delta z\Psi_S, \tag{7b}$$

where Ψ_S represents all terms on the right side of Eq. (1b). However, this method is a truly daunting and time-consuming calculation, it requires that Δz is equal to 1–5 μm. Simulating 1 μs of device operation would require 10^7 updates in time for each grid point on the axis of the laser. Consequently, we employ an accurate procedure for transferring the iterations step into a larger distance. Without affecting the accuracy, the iterative step size can be increased by 5 to 10 times. Considering an instantaneous moment, R and S have the following correlation[16]:

$$\frac{\mathrm{d}}{\mathrm{d}z}\begin{bmatrix}\bar{R}\\ \bar{S}\end{bmatrix} = \begin{bmatrix} g-a-\varepsilon & i\kappa-\varepsilon \\ -i\kappa+\varepsilon & -g+a+\varepsilon\end{bmatrix}\begin{bmatrix}\bar{R}\\ \bar{S}\end{bmatrix}. \tag{8}$$

According to the algorithm of differential matrix, the following results can be obtained:

$$\begin{bmatrix}\bar{R}(z+\Delta z)\\ \bar{S}(z+\Delta z)\end{bmatrix} = \exp(\tilde{M}\Delta z)\begin{bmatrix}\bar{R}(z)\\ \bar{S}(z)\end{bmatrix}, \tag{9}$$

where $\tilde{M}$ represents the matrix in Eq. (8). Similarly, let $\Delta z' = -\Delta z$, we can obtain the following relationships:

$$\begin{bmatrix}\bar{R}(z-\Delta z)\\ \bar{S}(z-\Delta z)\end{bmatrix} = \exp(\tilde{M}(-\Delta z))\begin{bmatrix}\bar{R}(z)\\ \bar{S}(z)\end{bmatrix}. \tag{10}$$

Let matrix $F = \exp(\tilde{M}\Delta z)$, matrix $B = \exp(\tilde{M}(-\Delta z))$, so:

$$\bar{R}_{m+1} = F_{11}\bar{R}_m + F_{12}\bar{S}_m, \tag{11a}$$

$$\bar{S}_{m-1} = B_{21}\bar{R}_m + B_{22}\bar{S}_m. \tag{11b}$$

Considering the effects of time and spontaneous emission, the final expression is obtained:

$$R_{m+1}^{k+1} = F_{11}R_m^k + F_{12}S_m^k + \Phi_R\Delta z, \tag{12a}$$

$$S_{m-1}^{k+1} = B_{21}R_m^k + B_{22}S_m^k + \Phi_S\Delta z. \tag{12b}$$

Boundary conditions:

$$R_{m=1} = r_{\mathrm{b}}S_{m=1}, \tag{13a}$$

Table 1. Parameters of simulation.

Parameter	Typical value
Back grating length (L_1)	100 μm
MO area length (L_2)	600 μm
Front grating length (L_3)	50, 75, 100, 200 μm
PA area length (L_4)	1200 μm
MO area width	4 μm
Front cavity width	134 μm
Current injection efficiency (η_i)	0.95
Spontaneous emission factor (n_{sp})	2.6
Differential gain coefficient (A)	1.0×10^{-11} cm
Transparency carrier density (N_0)	1.0×10^{12} cm^{-2}
Total recombination time (τ_e)	1.3×10^{-9} s
Grating cross coupling coefficient (κ)	30 cm^{-1}
Grating radiation loss (ε)	10 cm^{-1}
Approximately emission wavelength (λ)	980 nm
Front cavity facet power reflective (R_f)	0.002
Back cavity facet power reflective (R_b)	0.3
Group refractive index (n_g)	4.6
MO area injection current (I_{MO})	120 mA
PA area injection current (I_{PA})	3.0 A

$$S_{m=n} = r_f R_{m=n}, \tag{13b}$$

where n, r_f, r_b are the numbers of the last step size, the reflectivity of the front cavity surface and the reflectivity of the rear cavity surface, respectively.

The differential recurrence relationship of carriers is as follows:

$$N_m^{k+1} = N_m^k + \Delta t \cdot \Im, \tag{14}$$

where $\Im$ represents the right terms in Eq. (6), and $\Delta t = \dfrac{\Delta z}{v_g}$. Simultaneous Eqs. (12), (13) and (14) can be used to solve the carrier change and light field change in the device. It is suitable for grating-free Fabry-Perot tapered lasers, tapered lasers with DBR gratings and DFB lasers.

3. Simulation results and analysis

In an ideal case, the reflectivity of the front cavity facet of the amplifier is zero, which would only display system dynamics originating in the master oscillator. The tapered amplify region amplifies the mode produced by the master oscillator region. In practice, the reflectivity of the front cavity surface is not zero, which will introduce additional models and aggravate the mode competition. For the noise term[17, 18], each cyclic iteration produces the random number of Gaussian distribution with mean value of 0 and variance of 1, but must satisfy Eq. (4). The simulation parameters are shown in Table 1.

When the power reflectivity of the front-end face is 0.002 and the length of the front grating is 50 μm, as shown in Fig. 2, the carrier concentration of the device varies with time. In the first few nanoseconds, the carrier concentration rises sharply. The reason for this phenomenon is that the photons in the device have not yet been produced, and after the photons are excited, the carrier concentration decreases rapidly, and finally tends to be stable, and the generation of carriers and the transformation of photons reach a dynamic equilibrium. The following is the total number of photons in

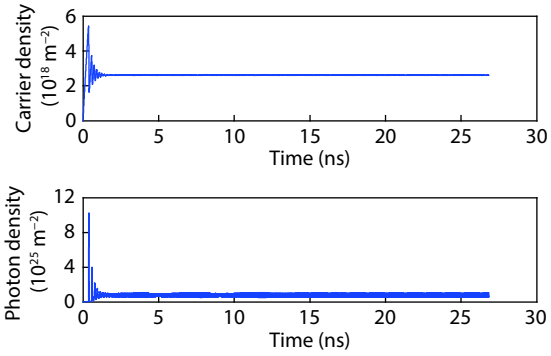

Fig. 2. (Color online) The top panel shows the change of total charge carriers and the bottom panel shows the change of total photons with the change of time with a 50 μm front grating.

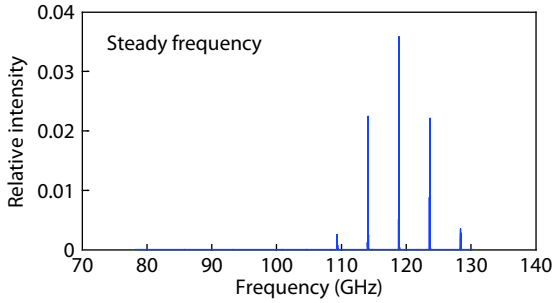

Fig. 3. (Color online) The frequency of output light with a 50 μm front grating.

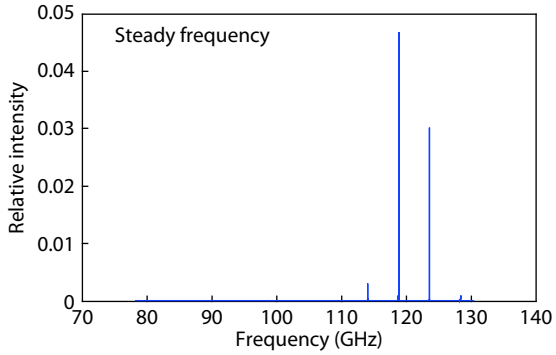

Fig. 4. (Color online) The frequency of output light when front grating is 75 μm.

the device, which tends to be stable after the initial rapid change, slightly lagging behind the change of carrier concentration. Fig. 3 shows the spectrum after Fourier transform of the output light field power. As can be seen, there are multiple longitudinal mode patterns whose spacings are about 50 GHz when the device works stably, displaying serious mode competition between longitudinal modes.

Lengthening the front grating L_3 can improve longitudinal mode characteristics. Increasing the front grating to 75 μm and the other conditions remain unchanged. It can be seen from the following figure that the number of longitudinal modes is obviously reduced, and the single longitudinal mode characteristics are more obvious with only three modes left, as shown in Fig. 4.

By extending the length of the grating L_3 to 100 μm, we observe that the laser has high power and excellent longitudinal mode characteristics. In the simulation, mode competi-

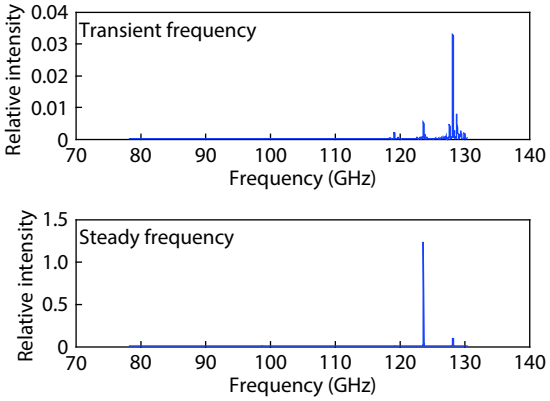

Fig. 5. (Color online) The top panel shows the transient frequency of output light during 0–5 ns and the bottom panel shows the stable state frequency of output light with a 100 μm front grating.

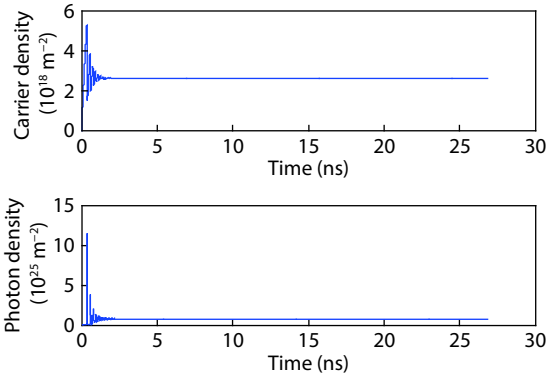

Fig. 6. (Color online) The top panel shows the change of total charge carriers and the bottom panel shows the total photons with a 100 μm front grating.

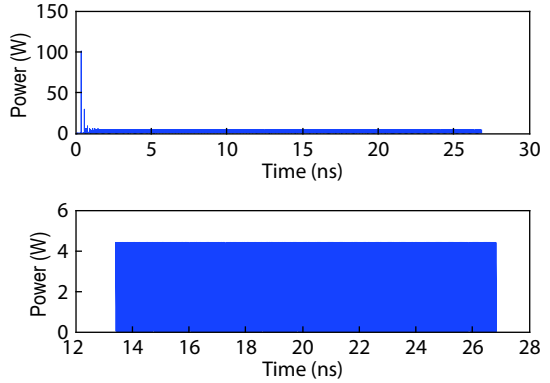

Fig. 7. (Color online) The top panel shows the change of output power with the change of time during all simulation time and the bottom panel shows the output power in stable state with a 100 μm front grating.

tion occurs only in the first few nanoseconds. During this time, the master oscillator settles into a single longitudinal mode. As shown in Fig. 5, the above is the spectrum of the initial unstable state, and the below is the stable output spectrum.

Fig. 6 shows the variation of carriers and photons under the condition that the length of the front grating L_3 is 100 μm. Fig. 7 shows the output power of the end facet, the output power above is the full time domain output power, and the bottom is the stable output power. As can be seen, under the stable condition, the output power tends to be

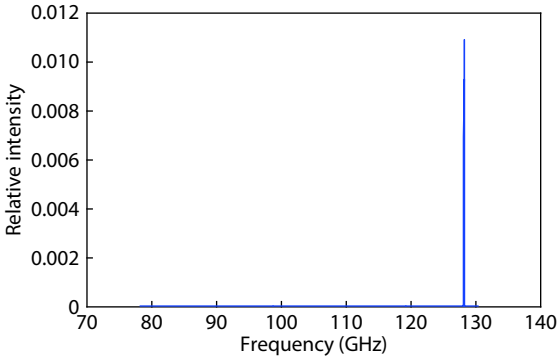

Fig. 8. (Color online) The stable state frequency of output light with a 200 μm front grating.

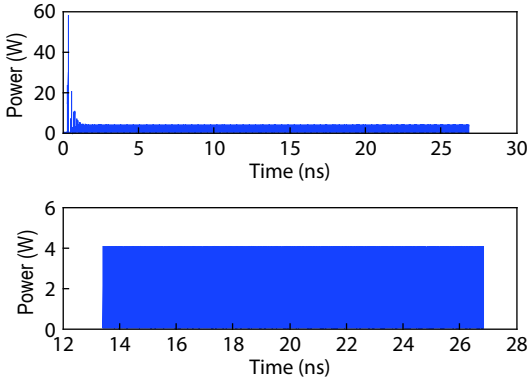

Fig. 9. (Color online) The top panel shows the change of output power with the change of time during all simulation time and the bottom panel shows the output power in stable state with a 200 μm front grating.

stable. When the front grating is continued to increase to 200 μm, there is almost one longitudinal mode in the device (as shown in Fig. 8) but the power of the output light field is slightly lower than that of the front grating is 100 μm (as shown in Fig. 9).

From these frequency figures it can be found that along with the increase of the length of the front grating, there are fewer and fewer stable modes in the device. When the front grating is extended to 100 μm, almost one longitudinal mode exists in the compound-cavity, for which the front grating with suitable length can eliminate the mode degeneracy and ensure the stable operation of the single mode in the device.

4. Conclusion

We use coupled-wave equation to accurately analyze model the single longitudinal mode and the multiple longitudinal mode in a compound cavity. The integration algorithms in Eq. (12) can help us to take larger time steps while maintaining computational efficiency and accuracy. To get nearly ideal single longitudinal mode and high-power output, we optimize the length of front gratings. When the front grating is extended to no less than 100 μm, mode competition occurs over only the first few nanoseconds, at which time the master oscillator settles into a single longitudinal mode. Meanwhile, considering that the structure scale of the laser must be controlled in a certain range and maintain its high photoelectric transformation efficiency, the grating length cannot be too long to avoid affecting its practicability. Therefore, the ideal light output can be obtained by in-

creasing the length of front grating to about 100 μm, when MO and PA area are driven separately using different electrodes[19].

The calculated results in this paper have significance for the actual fabrication of tapered lasers with DBR gratings. The model that we have developed in this article can be used to analyze 3D simulations when lateral and transverse optical fields are considered[20] and can then be used to simulate various types of semiconductor lasers, including DBR gratings, DFB gratings and so on[21, 22].

References

[1] Sun S M, Fan J, Xu L, et al. Research progress of conical semiconductor lasers. Chin Opt, 2019, 12(01), 48

[2] Zhou X Y, Zhao S Y, Ma X L, et al. Low vertical divergence angle high brightness photonic crystal semiconductor laser. Chin J Lasers, 2017, 44(2), 0201010

[3] Liu Y Q, Cao Y H, Li J, et al. 5 kW fiber coupled semiconductor laser for laser processing. Opt Prec Eng, 2015, 23(05), 1279

[4] Paschke K, Sumpf B, Dittmar F, et al. Nearly diffraction limited 980-nm tapered diode lasers with an output power of 7.7 W. IEEE J Sel Top Quantum Electron, 2005, 11(5), 1223

[5] Jia P, Liu X L, Chen Y Y, et al. Study of dual wavelength distributed Bragg reflection semiconductor laser with high order Bragg gratings. Chin J Lasers, 2015(8), 37

[6] Aho A T, Viheriälä J, M Korpijärvi V M, et al. High-power 1180-nm GaInNAs DBR laser diodes. IEEE Photonics Technol Lett, 2017, 29(23), 2023

[7] Fan J, Gong C Y, Yang J J, et al. Research progress of distributed prague reflector semiconductor lasers. Progr Laser Optoelectron, 2019, 56(06), 34

[8] Müller A, Fricke J, Bugge F, et al. DBR tapered diode laser with 12.7 W output power and nearly diffraction-limited, narrowband emission at 1030 nm. Appl Phys B, 2016, 122(4), 87

[9] Kogelnik H, Shank C V. Coupled-wave theory of distributed feedback lasers. J Appl Phys, 1972, 43(5), 2327

[10] Dente G C, Tilton M L. Modeling multiple-longitudinal-mode dynamics in semiconductor lasers. IEEE J Quantum Electron, 1998, 34(2), 325

[11] Hasler K H, Wenzel H, Klehr A, et al. Simulation of the generation of high-power pulses in the GHz range with three-section DBR lasers. IEE Proceedings-Optoelectronics, 2002, 149(4), 152

[12] Radziunas M. Modeling and simulations of broad-area edge-emitting semiconductor devices. Intl J High Perform Comput Appl, 2018, 32(4), 512

[13] Vahala K, Yariv A. Semiclassical theory of noise in semiconductor lasers-Part I. IEEE J Quantum Electron, 1983, 19(6), 1096

[14] Vahala K, A Yariv A. Semiclassical theory of noise in semiconductor lasers-Part II. IEEE J Quantum Electron, 1983, 19(6), 1102

[15] Zhang L M, Yu S F, Nowell M C, et al. Dynamic analysis of radiation and side-mode suppression in a second-order DFB laser using time-domain large-signal traveling wave model. IEEE J Quantum Electron, 1994, 30(6), 1389

[16] Dente G C, Tilton M L, Bossert D J, et al. Time-dependent modeling of the MFA-MOPA. In: Laser Diodes and Applications II. International Society for Optics and Photonics, 1996, 2682: 48

[17] De Melo A M, Petermann K. On the amplified spontaneous emission noise modeling of semiconductor optical amplifiers. Opt Commun, 2008, 281(18), 4598

[18] Marcuse D. Computer simulation of laser photon fluctuations: Theory of single-cavity laser. IEEE J Quantum Electron, 1984, 20(10), 1139

[19] Borruel L, Odriozola H, Tijero J M G, et al. Design strategies to increase the brightness of gain guided tapered lasers. Opt Quantum Electron, 2008, 40(2–4), 175

[20] Spreemann M, Lichtner M, Radziunas M, et al. Measurement and simulation of distributed-feedback tapered master-oscillator power amplifiers. IEEE J Quantum Electron, 2009, 45(6), 609

[21] Qiao C, Su R G, Li X, et al. Design and technology of 980 nm high power DBR semiconductor laser. Chin Laser, 2019, 46(7), 0701002

[22] Wang W X, Lu Y X. Analysis of sampling grating characteristics of distributed feedback semiconductor lasers. Laser J, 2018, 39(10), 57